Journal of Asian Earth Sciences 41 (2011) 31–43

Contents lists available at ScienceDirect

Journal of Asian Earth Sciences

journal homepage: www.elsevier.com/locate/jseaes

Geochemistry and geochronology of acidic rocks in the Beishan region, NW China: Petrogenesis and tectonic implications

Ben-Xun Su [a,b,*], Ke-Zhang Qin [a,*], Patrick Asamoah Sakyi [c], Ping-Ping Liu [d], Dong-Mei Tang [a], Sanjeewa P.K. Malaviarachchi [e], Qing-Hua Xiao [a], He Sun [a,b], Yu-Cai Dai [f], Yan Hu [b]

[a] Key Laboratory of Mineral Resources, Institute of Geology and Geophysics, Chinese Academy of Sciences, P.O. Box 9825, Beijing 100029, China
[b] State Key Laboratory of Lithospheric Evolution, Institute of Geology and Geophysics, Chinese Academy of Sciences, P.O. Box 9825, Beijing 100029, China
[c] Department of Earth Science, University of Ghana, P.O. Box LG 58, Legon-Accra, Ghana
[d] Department of Earth Sciences, The University of Hong Kong, Pakfulam Road, Hong Kong, China
[e] Research School of Earth Sciences, The Australian National University, Building 61, Mills Road Acton, Canberra, Act 0200, Australia
[f] No. 6 Geological Party, Xinjiang Bureau of Geology and Mineral Resources, Hami 839000, China

ARTICLE INFO

Article history:
Received 19 July 2010
Received in revised form 28 November 2010
Accepted 7 December 2010
Available online 14 December 2010

Keywords:
Beishan
Central Asian Orogenic Belt
Dacite
Magmatism
Rhyolite
Zircon U–Pb–Hf–O isotopes

ABSTRACT

The dacites and granites from the Beishan region are characterized by highly-fractionated REE, enrichments in LILE, and depletion in Nb, Ta and Sr. The dacites contain zircons with ages ranging from 265 to 748 Ma. These features suggest that they were probably derived from the older lower continental crust and were later on subjected to significant crustal assimilation. The rhyolites, diorites and diabases, all of which share similar geochemical features such as trace element patterns, zircon U–Pb ages of ~280 Ma, positive $\varepsilon_{Hf}(t)$ and $\varepsilon_{Nd}(t)$, high initial $(^{87}Sr/^{86}Sr)i$ and $\delta^{18}O‰$ values, were most likely derived from the juvenile crustal sources and subsequently experienced fractional crystallization and crustal contamination. These acidic igneous rocks (except dacites and granites) and coeval mafic–ultramafic intrusions form a bimodal igneous series. This implies that the Beishan region was a Late Paleozoic rift probably developed in association with the early Permian mantle plume activity in the Tarim Basin.

1. Introduction

The Eastern Tianshan and Beishan, situated in the southern margin of the Central Asian Orogenic Belt (CAOB), is a conjunction region of the CAOB, Sino-Korean and Tarim cratons (Fig. 1A). Since large volumes of Paleozoic volcanic and plutonic rocks are distributed there (Fig. 1B; Gu et al., 2001; Qin et al., 2002, 2003; Han et al., 2004; Zhou et al., 2004; Jiang et al., 2006; Wang et al., 2006; Tang et al., 2009; Li et al., 2010a), it has been considered as an important region to investigate the tectonic evolution of the CAOB (Yue et al., 2001; Han et al., 2006; Li et al., 2006a,b; Mao et al., 2008; Pirajno et al., 2008; Xu et al., 2009; Ao et al., 2010; Su et al., 2010a,b). Most of the studies on this region have been focused on the rocks in the Eastern Tianshan, while those of the Beishan region have received little attention, in part due to the general lack of accessibility and the extreme climatic conditions prevailing in the region. The tectonic framework of the Beishan region in the Late Paleozoic, which is critical in understanding the subduction and closure of the South Tianshan Ocean, as well as the orogenic process of the southern margin of the CAOB, has remained a controversial issue. Based on the inferred occurrence of Alaskan-type complex, some proposed that the Beishan region represents an arc setting in Late Paleozoic (Mao, 2008; Xiao et al., 2009; Ao, 2010; Ao et al., 2010). However, more authors preferred an intra-continental rift setting (Xiao et al., 2000, 2004a; Jiang et al., 2006; Yang et al., 2008; Xu et al., 2009). But at present, they still have not got sufficient evidence, including the absence of bimodal igneous series, to support their opinion.

Tectonic setting could be inferred from rock assemblages and their geochemical characteristics. The mafic–ultramafic intrusions in the Beishan region are construed to be derived from the upper mantle (Li et al., 2006a; Jiang et al., 2006; Mao et al., 2008; Pirajno et al., 2008; Yang et al., 2008; Su et al., 2009, 2010a,c). Even though these rocks contain a wealth of information about petrogenetic evolution and related magmatic processes, few geochemical and geochronological works have been done on them. Furthermore, the acidic rocks, such as rhyolite, granite and dacite, have not yet been investigated in detail. For these reasons, the petrogenetic relationship between the acidic rocks and the mafic–ultramafic intrusions is poorly known. In this contribution, we present the geochemical and Sr–Nd isotopic compositions and zircon U–Pb–Hf–O data of volcanic rocks and related intrusive rocks from

* Corresponding authors. Address: State Key Laboratory of Lithospheric Evolution, Institute of Geology and Geophysics, Chinese Academy of Sciences, P.O. Box 9825, Beijing 100029, China (B.-X. Su). Tel.: +86 10 82998514; fax: +86 10 62010846.
E-mail addresses: subenxun@mail.igcas.ac.cn (B.-X. Su), kzq@mail.igcas.ac.cn (K.-Z. Qin).

1367-9120/$ - see front matter © 2010 Elsevier Ltd. All rights reserved.
doi:10.1016/j.jseaes.2010.12.002

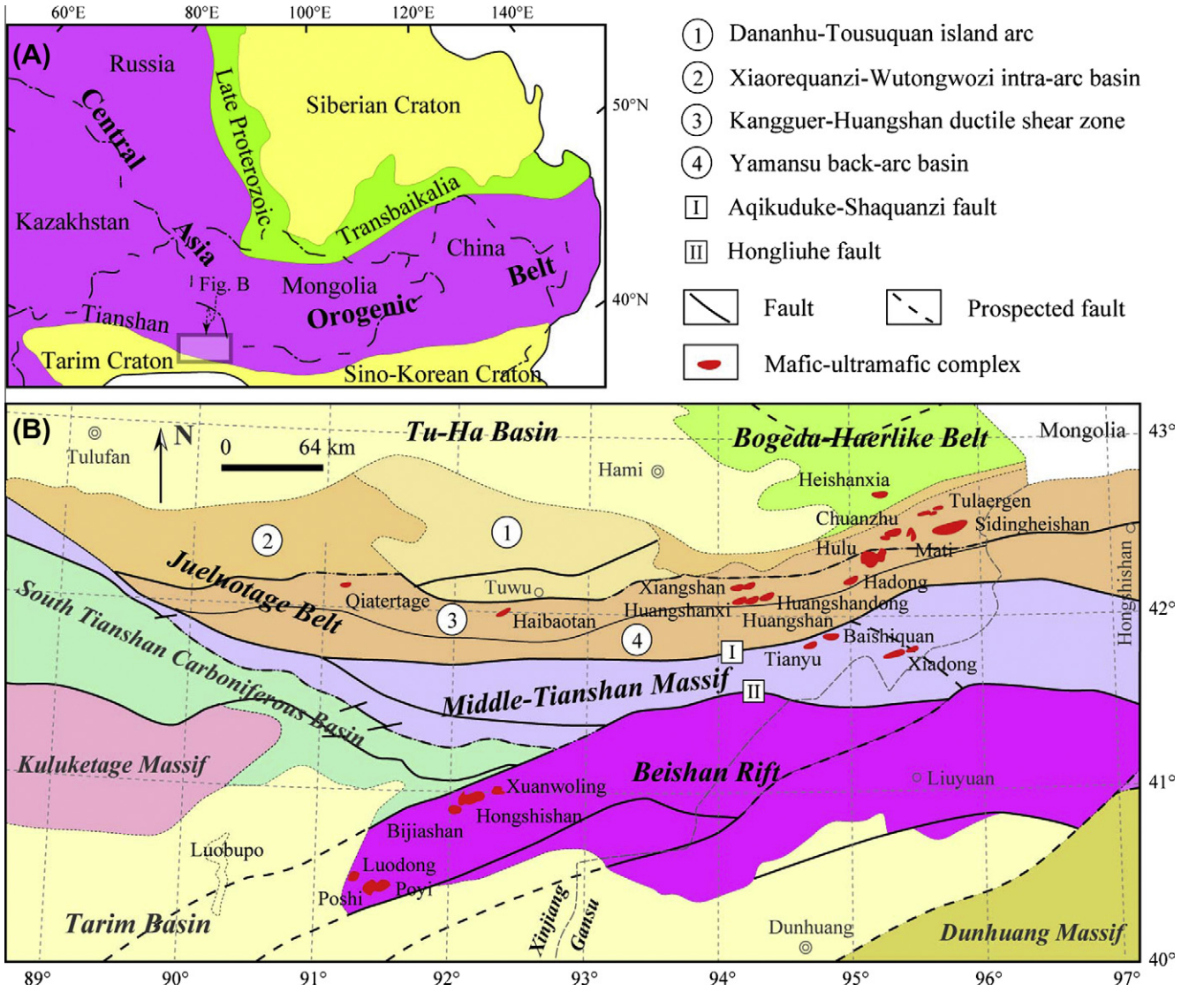

Fig. 1. (A) A geologic map of the study area, showing the location of the Siberian, Tarim and Sino-Korean Cratons in relation to the Central Asian Orogenic Belt (modified after Jahn et al. (2000)). (B) Regional geological map of the Eastern Tianshan and Beishan regions showing the distribution of Paleozoic mafic–ultramafic complexes (Su et al., 2010b).

the Beishan region to decipher their evolutional history such as petrogenesis and tectonic implications.

2. Geological background and sampling

The Beishan region is located in the northeastern part of the Tarim basin, adjacent to the Middle Tianshan Massif in the north (Fig. 1B; BGMRXUAR, 1993; Xu et al., 2009). It is mainly comprised of Precambrian crystalline basement and overlying sedimentary rocks, which include the Beishan, Gutongjing, Yangjibulake and Aierlanjigan groups. The Precambrian to Permian strata in the Beishan region are separated by well-developed fault-related uplifts and sags (Yue et al., 2001; Xu et al., 2009; Su et al., 2010c). Late Paleozoic tectonic history in this region is closely related to the subduction and subsequent closure of the South Tianshan Ocean, the latter process being described as quite complicated (e.g., Gao et al., 1998, 2006, 2009; Yue et al., 2001; Zhang et al., 2002; Xiao et al., 2009, 2010a). Previous geochronological studies on ophiolites (320–440 Ma; Wang et al., 1998; Long et al., 2006 and references therein) in the western Tianshan indicate that the South Tianshan Ocean in the west was closed in early Carboniferous. The youngest ophiolite reported in the Beishan region is 420 Ma in age, and Hf model ages of most mantle-derived rocks are older than 400 Ma (Mao, 2008; Ao, 2010), indicating that the closure of the South Tianshan Ocean in the east was around 400 Ma. Therefore, it is possible that the closure of the South Tianshan Ocean was a scissor-like process, which commenced in the east and ended in the west.

The Permian mafic–ultramafic complexes discovered so far are mainly distributed in the western part of the Beishan region and intrude the Proterozoic and Carboniferous strata (BGMRXUAR, 1993; Jiang et al., 2006; Su et al., 2009; Xu et al., 2009). From west to east, the mafic–ultramafic intrusions are distributed as follows: Luodong, Poshi, Poyi, Bijiashan, Hongshishan and Xuanwoling, and have been successively explored in the past decades (Fig. 1B; Xiao et al., 2000, 2004a; Jiang et al., 2006; Li et al., 2006a; Yang et al., 2008; Su et al., 2009, 2010a,c; Ao et al., 2010). They are dominated by dunite, clinopyroxene peridotite, troctolite and gabbro. The Proterozoic quartz diorites are intruded by the Poshi and Poyi complexes, while other complexes have country rocks of mainly Carboniferous biotite–quartz schist (Jiang et al., 2006; Li et al.,

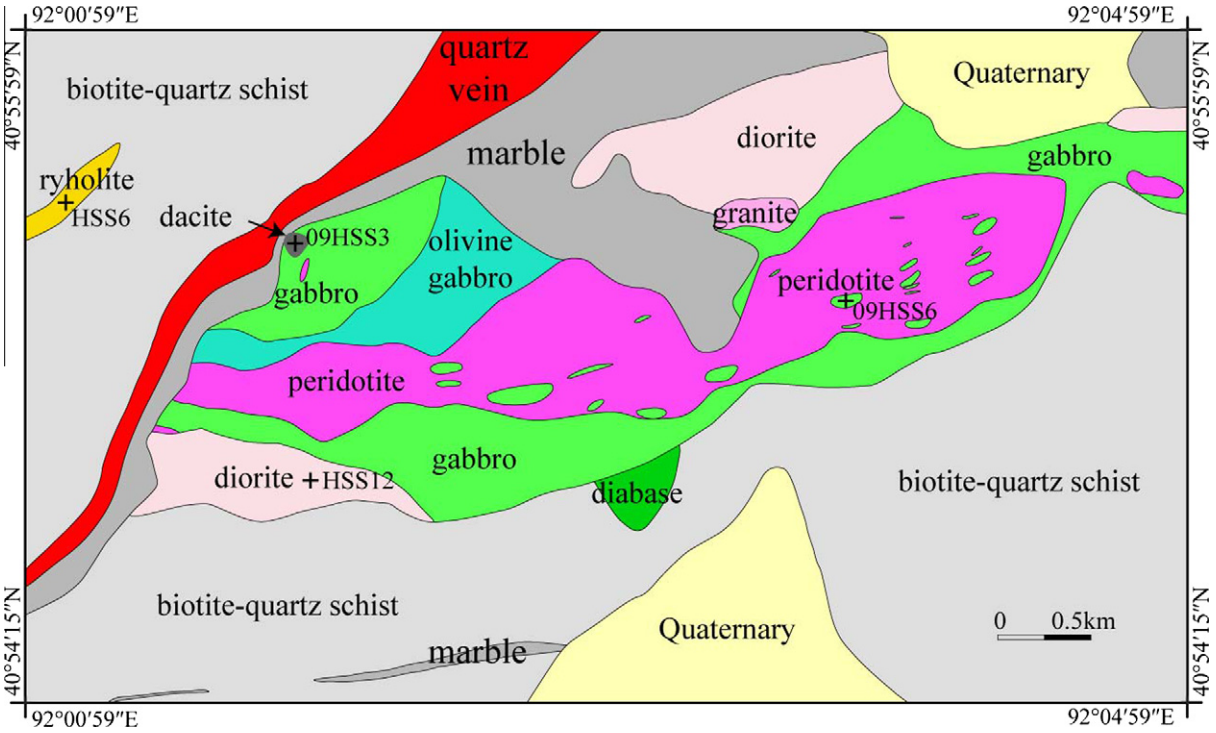

Fig. 2. Simplified geological map of the Hongshishan mafic–ultramafic intrusion showing the distribution of volcanic rocks and sampling positions (modified after Su et al. (2009)).

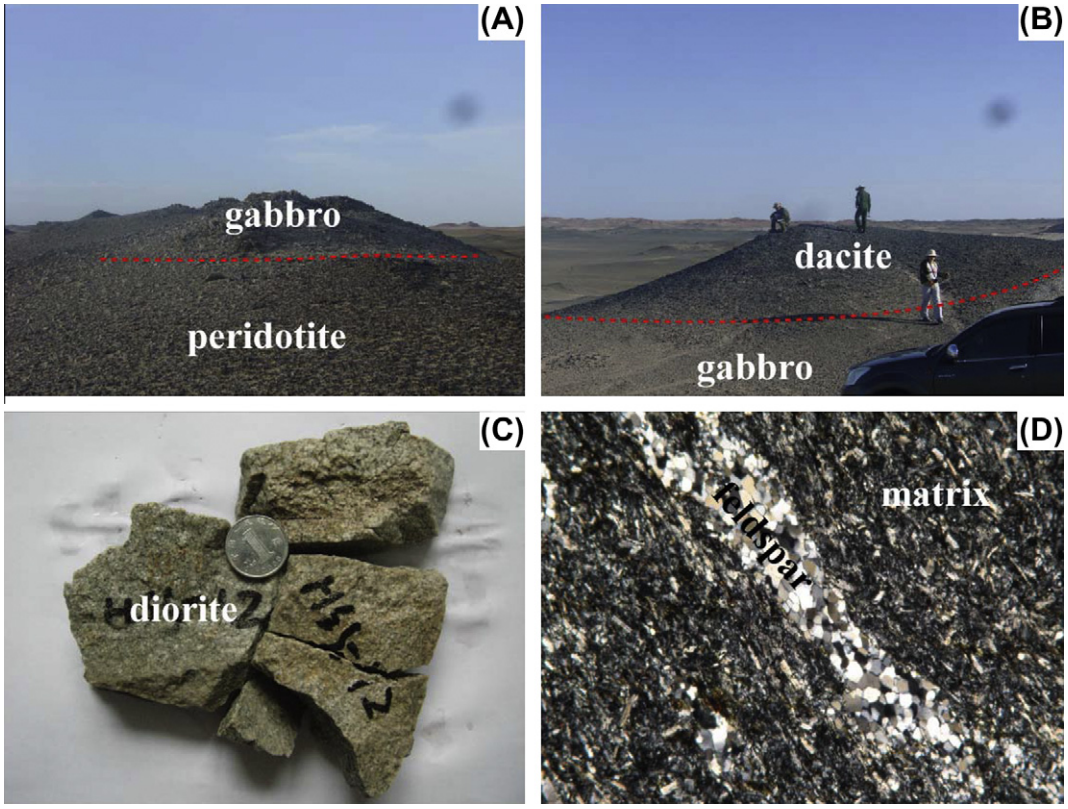

Fig. 3. Occurrence and petrography of the studied rocks from the Hongshishan area. (A) Gabbro massif above the peridotite; (B) Dacite occurs above the gabbro; (C) Diorite shows silicified feature; (D) Rhyolite shows feldspar phenocrysts in the matrix.

2006a; Su et al., 2009, 2010c). Diorite, marble, granite and diabase veins occasionally surround or occur within the intrusions (Fig. 2; Jiang et al., 2006; Su et al., 2009, 2010a,c).

Some gabbro massifs and dacites occur, like floating, above the peridotite and gabbro of the Hongshishan intrusion with sharp contacts (Figs. 2 and 3A and B), appearing to have no petrogenetic

affinity to the main mafic–ultramafic body. Mineralogically, the dacites have plagioclase phenocrysts and matrix with mineral assemblage of plagioclase, quartz and hornblende. The diorites from the Hongshishan and Luodong areas consist of hornblende, plagioclase and quartz, with the Hongshishan diorite displaying silicified characteristics in hand-specimen (Fig. 3C). Outcrops of rhyolites in the west of the Hongshishan intrusion cover the Carboniferous biotite–quartz schist. The rhyolites are moderately phyric rocks with phenocrysts of sanidine, quartz and feldspar in a glassy matrix of fine-grained quartz and feldspar (Fig. 3D). The biotite–quartz schist and diabase were sampled from the Bijiashan intrusion, while the biotite-plagioclase granite and potassic granite samples were collected from the country rocks hosting the Xuanwoling intrusion (Su et al., 2010a).

3. Analytical methods

The major and trace element results are listed in Table 1. The Rb–Sr and Sm–Nd isotopic data are given in Table 2. Zircon U–Pb isotopic data and Hf-O isotopic data are presented in Table 3 and 4, respectively.

3.1. Major and trace elements

Analyses of major and trace element abundances of all 14 samples were carried out at the Institute of Geology and Geophysics, Chinese Academy of Sciences. Major elements were determined using Shimadzu X-ray fluorescence (XRF-1500) on fused glass beads. Analytical uncertainties were 1–3% relative to elements present in concentrations >1 wt.%, and about 10% relative to elements present in concentrations <1 wt.%. Trace elements were determined by inductively coupled plasma mass spectrometry (ICP-MS) using an Agilent 7500a system. Samples were digested using a mixture of ultra-pure HF and HNO_3 in Teflon bombs. Analytical procedures are described in detail by Chu et al. (2009). Precisions of the ICP-MS analyses were generally better than 5%.

3.2. Sr–Nd isotope

Rb–Sr and Sm–Nd isotopic analyses were performed on a VG-354 thermal ionization magnetic sector mass spectrometer at the Institute of Geology and Geophysics, Chinese Academy of Sciences. Procedures of chemical separation and isotopic analyses followed that of Zhang et al. (2001). Mass fractionation corrections for Sr and Nd isotopic ratios were based on $^{86}Sr/^{88}Sr$ and $^{146}Nd/^{144}Nd$ values of 0.1194 and 0.7219, respectively. Uncertainties of Rb/Sr and Sm/Nd ratios were less than 2% and 0.5%, respectively.

3.3. Zircon U–Pb–Hf–O isotopes

Zircon grains were separated using conventional heavy fraction and magnetic techniques. Together with zircon standard TEMORA, they were mounted in epoxy and then polished to expose the crystals, possibly halfway, for analysis. Thereafter, all the zircons were photographed in transmitted and reflected lights, and cathodoluminescence (CL) images were obtained to identify and examine the analyzed grains. The mounts were then vacuum-coated with high-purity gold. U–Pb-O isotopes were measured using Cameca IMS 1280 large-radius SIMS. Detailed working conditions and analytical procedures were described elsewhere (Li et al., 2009, 2010b). The internal precision of a single analysis was generally better than 0.2‰ for $^{18}O/^{16}O$ ratio. Lu–Hf isotopes were determined using laser-ablation multi-collector inductively coupled plasma mass spectrometry (LA-ICP-MS). The detailed analytical procedures are described in Wu et al. (2006) and Li et al. (2010b). All analyses were carried out at the Institute of Geology and Geophysics, Chinese Academy of Sciences.

4. Analytical results

4.1. Major element

The volcanic rocks from the Hongshishan area can be divided into two types: rhyolites and dacites (Fig. 4). The compositional range of major elements in the rhyolites are as follows: SiO_2 (70.3–72.1 wt.%), TiO_2 (0.68–0.76 wt.%), Al_2O_3 (12.5–12.8 wt.%), TFeO (total Fe, 2.61–2.94 wt.%), K_2O (2.34–2.93 wt.%) and Na_2O (4.96–5.43 wt.%) (Table 1; Fig. 5). In contrast, the dacites show relatively lower SiO_2 (66.3–67.6 wt.%) and Na_2O (0.93–1.06 wt.%), and higher Al_2O_3 (14.8–15.1 wt.%), TFeO (4.75–5.02 wt.%) and K_2O (5.68–6.21 wt.%) contents (Fig. 5). Compared with the fresh diorite sample (LD-δ), the silicified one (HSS12) has significantly higher SiO_2 content but lower contents of other oxides (Table 1; Fig. 5). The granites and biotite–quartz schist possess very similar major element compositions. The diabase has relatively higher TiO_2 and TFeO, and lower SiO_2 and K_2O contents. These rocks do not show any obvious compositional correlation (Fig. 5).

4.2. Trace element

The dacites and granites show very similar trace element patterns. They have highly-fractionated rare earth element (REE) patterns with negative Eu anomalies (Fig. 6A). In spider diagram, they are rich in large ion lithophile element (LILE) such as Rb, Ba, Th, U and Pb, depleted in high strength field element (HSFE) such as Nb, Ta and Ti, and slightly depleted in Zr and Hf (Fig. 6B). The rhyolites exhibit weakly fractionated REE patterns with apparently negative Eu anomaly (Fig. 6C). They are characterized by positive Th, U, Pb, Zr and Hf anomalies, and negative Nb, Ta, Sr and Ti anomalies (Fig. 6D). The diorite, diabase and biotite–quartz schist display near-identical REE and trace element patterns to the rhyolites, but can be distinguished from them by their relatively lower trace element abundances and variable LREE contents (Fig. 6C and D). Contrastingly, the mafic–ultramafic intrusions from the Beishan region are marked by lower trace element abundances, flat REE patterns with positive Eu anomalies, slight enrichments in Rb, U and Sr, and depletion in HFSE (Fig. 6E and F; Jiang et al., 2006; Su et al., 2010a,c).

4.3. Sr–Nd isotope

The Hongshishan diorite (HSS12) shows high $(^{87}Sr/^{86}Sr)i$ of 0.71012 and low $\varepsilon_{Nd}(t)$ of −1.8 (Table 2). The rhyolites have $(^{87}Sr/^{86}Sr)i$ ratios in the range of 0.70644 to 0.70663 and $\varepsilon_{Nd}(t)$ ranging from +2.6 to +4.3 (Fig. 7). The two dacite samples are characterized by very high $^{87}Sr/^{86}Sr$ (0.778037 and 0.777534) and low $^{143}Nd/^{144}Nd$ (0.511856 and 0.511764) respectively, but their initial ratios could not be calculated due to the lack of concordia zircon U–Pb age (Table 2).

4.4. Zircon U–Pb age and Hf–O isotope

The CL images of representative zircons are shown in Fig. 8. The Hongshishan rhyolite (HSS6) contains equant to short, prismatic zircons. They are colorless and transparent to translucent and range in length from 60 to 100 μm, with length/width ratios of 1:1–1.5:1. The equant grains display regular concentric zoning with bright luminescence, while the short prismatic grains have oscillatory or patchy zonation with low luminescence (Fig. 8). The U and Th concentrations of these zircons are 186–813 ppm

Table 1
Major (wt.%) and trace (ppm) elements of volcanic and plutonic rocks in the Beishan region.

Sample	HSS6-1	HSS6-2	HSS6-3	HSS6-4	09HSS3-1	09HSS3-2	09HSS3-3	09HSS3-4	HSS12	BJS-11	BJS-14	XWL7	XWL-r	LD-δ
Rock type	Rhyolite	Rhyolite	Rhyolite	Rhyolite	Dacite	Dacite	Dacite	Dacite	Silicified diorite	Bio-Qtz schist	Diabase	Bio-Pl granite	Potassic granite	Diorite
SiO_2	71.6	70.3	72.1	71.5	67.6	66.7	66.6	66.3	74.7	72.3	55.2	75.8	72.5	57.2
TiO_2	0.74	0.76	0.74	0.68	0.76	0.78	0.77	0.78	0.34	0.43	1.44	0.19	0.17	1.21
Al_2O_3	12.5	12.8	12.5	12.6	14.8	15.0	15.0	15.1	13.5	13.4	14.6	12.5	14.0	15.3
Fe_2O_3	1.68	1.96	1.99	1.71	3.37	4.47	3.84	3.41	0.26	3.06	10.4	1.92	1.94	1.75
FeO	1.08	1.16	0.94	1.10	1.69	0.84	1.44	1.92	0.67					9.25
MnO	0.05	0.06	0.05	0.05	0.05	0.04	0.04	0.04	0.02	0.03	0.15	0.02	0.02	0.15
MgO	0.76	1.02	0.82	0.75	2.54	2.34	2.44	2.50	1.11	0.74	5.03	0.30	0.30	6.78
CaO	1.41	1.89	1.40	1.56	0.53	0.37	0.47	0.35	2.68	1.82	8.73	1.19	1.38	2.20
Na_2O	5.43	5.25	5.20	4.96	1.06	0.96	0.97	0.93	4.60	3.35	2.86	2.89	3.68	1.60
K_2O	2.49	2.34	2.41	2.93	5.68	5.87	5.82	6.21	0.60	3.90	0.42	4.31	4.68	0.09
P_2O_5	0.17	0.17	0.17	0.16	0.09	0.09	0.10	0.11	0.05	0.06	0.16	0.03	0.02	0.09
LOI	0.68	0.68	0.54	0.60	1.70	1.98	2.26	1.94	1.18	0.68	1.10	0.32	0.68	2.75
TOTAL	98.6	98.4	98.8	98.5	99.9	99.4	99.7	99.6	99.7	99.9	100.0	99.4	99.3	98.4
TFeO	2.61	2.94	2.75	2.66	4.75	4.90	4.92	5.02	0.91	2.75	9.39	1.73	1.75	10.83
$Na_2O + K_2O$	7.92	7.59	7.61	7.89	6.74	6.83	6.79	7.14	5.20	7.25	3.28	7.20	8.36	1.69
Li	2.74	3.19	0.19	3.00	45.9	34.6	38.7	52.9	1.66	6.43	6.41	5.26	5.47	27.5
Be	2.59	2.13	2.02	2.13	3.23	2.28	2.09	2.12	3.30	2.05	1.14	1.36	2.17	2.77
Sc	11.4	10.9	7.77	9.72	11.3	10.2	10.2	10.0	4.17	6.74	37.3	6.47	6.44	33.9
V	32.5	31.9	26.9	37.4	62.4	64.8	61.6	63.2	34.4	45.3	261	16.4	12.5	304
Cr	6.80	10.0	7.49	8.83	70.5	69.1	66.4	60.2	2.75	9.60	27.6	6.30	8.74	263
Co	4.87	4.49	4.73	4.84	16.2	17.7	16.4	15.7	6.94	7.12	35.8	2.99	1.45	34.1
Ni	4.06	4.51	2.84	3.55	24.9	22.2	24.1	24.1	25.5	6.40	15.4	6.40	3.48	122
Cu	6.75	3.78	3.90	7.26	4.49	3.72	3.19	4.58	28.0	4.76	28.5	11.2	4.09	22.8
Zn	87.8	48.3	49.9	50.9	102	59.5	62.7	91.7	19.0	22.1	58.7	26.7	23.2	185
Ga	17.9	17.4	15.7	18.7	21.7	20.8	21.3	21.1	14.1	18.5	18.7	16.7	18.6	23.7
Rb	45.1	42.3	43.1	38.0	193	175	183	191	31.3	124	16.8	127	154	3.57
Sr	53.8	66.1	54.7	63.2	73.7	75.7	67.0	69.0	148	105	179	116	107	130
Y	80.4	80.1	72.9	74.4	19.4	17.6	22.4	24.2	29.0	38.7	35.2	21.2	28.1	26.8
Zr	543	568	554	446	129	114	125	151	258	240	140	201	156	195
Nb	11.9	12.5	12.1	10.9	19.2	18.2	20.1	18.8	11.8	8.18	6.01	7.08	8.43	14.9
Cs	1.22	1.62	1.44	1.61	14.7	9.49	9.65	10.8	1.24	3.34	1.80	1.61	3.42	2.35
Ba	292	280	289	403	882	651	703	681	176	611	129	1601	1437	47.0
La	32.2	30.5	28.9	27.0	51.3	45.6	49.7	50.4	18.1	33.6	14.2	67.1	72.0	32.5
Ce	75.8	73.9	70.8	64.2	91.8	84.8	85.8	91.4	44.3	70.2	31.4	124	129	58.9
Pr	10.4	9.95	9.36	9.01	11.5	9.56	10.8	11.4	4.19	7.84	4.24	13.2	13.1	7.14
Nd	45.6	43.8	41.7	40.7	42.4	33.8	40.7	43.0	15.0	28.9	19.0	48.0	45.2	26.2
Sm	11.2	11.0	10.1	10.6	7.46	5.58	6.94	7.81	3.31	6.02	5.03	7.52	7.02	5.13
Eu	2.39	2.01	2.02	1.97	1.35	1.04	1.30	1.42	0.60	0.93	1.43	1.60	1.37	1.16
Gd	12.9	12.5	11.7	11.7	6.00	4.66	5.73	6.37	3.65	5.65	5.26	6.30	6.31	4.38
Tb	2.34	2.24	2.11	2.13	0.91	0.77	0.90	1.01	0.70	1.04	0.96	0.86	0.94	0.75
Dy	15.4	14.9	13.6	14.2	4.39	3.76	4.61	5.10	4.94	6.65	6.33	4.68	5.39	4.85
Ho	3.39	3.32	3.02	3.15	0.71	0.64	0.79	0.90	1.11	1.48	1.39	0.87	1.08	1.10
Er	9.44	9.24	8.56	8.82	1.86	1.76	2.16	2.48	3.27	4.16	4.00	2.29	2.88	3.27
Tm	1.41	1.40	1.30	1.33	0.28	0.26	0.32	0.37	0.52	0.64	0.62	0.33	0.42	0.52
Yb	9.17	9.07	8.44	8.45	1.57	1.49	1.96	2.32	3.47	4.27	4.04	2.09	2.75	3.70
Lu	1.40	1.40	1.31	1.30	0.24	0.27	0.29	0.31	0.53	0.65	0.60	0.32	0.41	0.62
Hf	14.2	14.4	14.6	13.2	3.37	2.52	2.88	3.21	8.04	7.87	4.32	6.11	5.54	6.08
Ta	0.97	0.98	0.98	0.91	1.59	1.54	1.70	1.54	2.23	0.84	0.49	0.45	0.67	1.15
Tl	0.17	0.16	0.17	0.15	0.83	0.70	0.72	0.80	0.23	0.42	0.13	0.73	0.71	
Pb	9.51	6.69	6.49	7.88	24.6	17.9	17.4	20.5	14.6	7.50	4.11	17.8	17.7	8.29
Bi	0.07	0.09	0.10	0.22	0.33	0.22	0.22	0.25	0.06	0.04	0.06	0.15	0.12	
Th	12.8	12.8	11.6	11.8	19.9	17.8	18.7	18.2	25.2	22.8	5.47	20.5	22.3	10.9
U	3.20	3.23	3.24	2.94	1.11	0.85	0.91	1.12	4.15	3.27	1.16	1.76	2.95	1.81

Note: Bio, biotite; Qtz, quartz; Pl, plagioclase.

Table 2
Sr–Nd isotopic compositions of volcanic and plutonic rocks in the Beishan region.

Sample	Rb (ppm)	Sr (ppm)	$^{87}Rb/^{86}Sr$	$^{87}Sr/^{86}Sr$	$2\sigma_m$	$(^{87}Sr/^{86}Sr)_i$	Sm (ppm)	Nd (ppm)	$^{147}Sm/^{144}Nd$	$^{143}Nd/^{144}Nd$	$2\sigma_m$	$(^{143}Nd/^{144}Nd)i$	$\varepsilon_{Nd}(t)$
HSS12	25.9	131	0.572	0.712445	0.000061	0.71012	3.03	14.1	0.1305	0.512424	0.000012	0.512180	-1.8
HSS6-1	42.3	73.9	1.66	0.713204	0.000100	0.70663	11.1	41.5	0.1616	0.512707	0.000019	0.512412	+2.6
HSS6-2	39.1	67.2	1.68	0.713221	0.000047	0.70655	11.6	43.0	0.1627	0.512793	0.000022	0.512496	+4.3
HSS6-3	39.2	55.3	2.05	0.714581	0.000031	0.70644	11.3	41.4	0.1657	0.512763	0.000005	0.512460	+3.5
HSS6-4	358	671	1.54	0.712693	0.000048	0.70658	10.0	37.1	0.1633	0.512730	0.000010	0.512432	+3.0
09HSS3-1	198	62.2	9.29	0.778037	0.000012		12.3	83.5	0.08929	0.511856	0.000006		
09HSS3-3	189	60.6	9.07	0.777534	0.000019		9.09	58.5	0.09392	0.511764	0.000015		

Note: Initial isotopic ratios are calculated based on their zircon U–Pb age. The re-calculation is not done on the dacite samples (09HSS3-1 and 09HSS3-3) due to lack of zircon concordia U–Pb age.

Table 3
U–Pb isotopic data of zircons from volcanic and plutonic rocks in the Beishan region.

Sample@spot	U (ppm)	Th (ppm)	Pb (ppm)	Th/U	$^{207}Pb/^{206}Pb$	±σ (%)	$^{207}Pb/^{235}U$	±σ (%)	$^{206}Pb/^{238}U$	±σ (%)	$t_{207/206}$ (Ma)	±σ	$t_{207/235}$ (Ma)	±σ	$t_{206/238}$ (Ma)	±σ
Rhyolite																
HSS6@1	225	123	12.0	0.55	0.0505	1.98	0.304	2.49	0.0436	1.50	217.6	45.3	269.2	5.9	275.2	4.0
HSS6@2	636	555	37.8	0.87	0.0506	1.52	0.315	2.14	0.0451	1.50	220.8	34.8	277.8	5.2	284.6	4.2
HSS6@3	724	618	41.5	0.85	0.0513	1.16	0.307	1.90	0.0434	1.50	254.7	26.3	271.9	4.5	274.0	4.0
HSS6@4	484	485	28.9	1.00	0.0521	1.45	0.314	2.09	0.0437	1.50	290.8	32.9	277.4	5.1	275.8	4.1
HSS6@5	186	89.7	10.0	0.48	0.0524	2.43	0.324	2.93	0.0448	1.64	302.8	54.4	284.6	7.3	282.4	4.5
HSS6@6	813	863	50.7	1.06	0.0530	1.60	0.330	2.21	0.0451	1.52	330.4	36.0	289.3	5.6	284.3	4.2
HSS6@7	346	237	19.2	0.68	0.0515	1.78	0.312	2.34	0.0440	1.51	262.0	40.4	275.7	5.7	277.3	4.1
HSS6@8	659	503	38.1	0.76	0.0524	1.17	0.323	1.90	0.0448	1.50	302.6	26.3	284.5	4.7	282.3	4.1
Dacite																
09HSS3@1	147	118	8.08	0.80	0.0495	3.62	0.287	3.94	0.0420	1.58	172.1	82.3	255.9	9.0	265.1	4.1
09HSS3@2	235	272	19.3	1.16	0.0515	3.65	0.421	3.96	0.0593	1.53	263.5	81.6	356.7	12.0	371.2	5.5
09HSS3@5	103	74.1	8.42	0.72	0.0584	4.88	0.522	5.11	0.0647	1.52	546.1	103.2	426.2	18.0	404.3	6.0
09HSS3@6	190	150	15.0	0.79	0.0554	2.67	0.471	3.08	0.0617	1.54	428.9	58.5	392.2	10.1	386.0	5.8
09HSS3@7	435	161	22.8	0.37	0.0525	2.84	0.329	3.23	0.0454	1.54	307.8	63.5	288.7	8.2	286.3	4.3
09HSS3@8	431	201	25.0	0.47	0.0536	1.83	0.361	2.38	0.0488	1.52	355.3	40.8	312.6	6.4	306.9	4.6
09HSS3@9	449	293	26.4	0.65	0.0532	1.84	0.347	2.39	0.0473	1.52	339.4	41.2	302.6	6.3	297.9	4.4
09HSS3@10	323	92.1	24.0	0.28	0.0560	2.49	0.504	2.95	0.0652	1.58	452.4	54.4	414.1	10.1	407.3	6.2
09HSS3@11	391	633	31.9	1.62	0.0531	1.84	0.396	2.39	0.0541	1.52	333.7	41.1	338.8	6.9	339.5	5.0
09HSS3@12	235	146	14.0	0.62	0.0512	3.46	0.341	3.79	0.0483	1.55	251.1	77.6	298.0	9.8	304.0	4.6
09HSS3@13	260	316	23.2	1.22	0.0555	2.36	0.488	2.81	0.0637	1.53	434.2	51.7	403.4	9.4	398.0	5.9
09HSS3@14	511	153	39.9	0.30	0.0552	1.70	0.518	2.29	0.0681	1.53	418.7	37.4	423.9	8.0	424.9	6.3
09HSS3@15	58.4	31.9	3.28	0.55	0.0540	6.79	0.350	6.98	0.0470	1.62	371.1	146.1	304.7	18.6	296.1	4.7
09HSS3@16	272	99.0	14.9	0.36	0.0500	2.95	0.328	3.33	0.0475	1.54	196.4	67.1	287.7	8.4	299.1	4.5
09HSS3@17	358	216	19.3	0.60	0.0528	2.10	0.321	2.60	0.0441	1.54	320.7	47.1	282.6	6.4	278.0	4.2
09HSS3@18	72.3	78.1	12.3	1.08	0.0652	2.60	1.106	3.02	0.1231	1.52	779.5	53.8	756.2	16.2	748.4	10.8
Diorite																
HSS12@1	1536	1389	90.6	0.90	0.0508	1.83	0.308	2.37	0.0439	1.50	229.9	41.8	272.3	5.7	277.2	4.1
HSS12@2	1066	1238	68.3	1.16	0.0517	0.95	0.323	1.78	0.0453	1.50	272.7	21.7	284.0	4.4	285.4	4.2
HSS12@3	210	114	11.4	0.54	0.0551	2.01	0.337	2.51	0.0444	1.52	415.0	44.2	294.8	6.5	279.9	4.2
HSS12@4	431	411	25.9	0.95	0.0520	1.65	0.320	2.23	0.0446	1.50	286.7	37.4	281.6	5.5	281.0	4.1
HSS12@5	396	232	21.9	0.59	0.0489	1.63	0.304	2.22	0.0450	1.51	143.5	37.8	269.1	5.3	283.8	4.2
HSS12@6	954	947	59.1	0.99	0.0532	1.21	0.333	1.93	0.0454	1.50	338.3	27.1	291.9	4.9	286.2	4.2
HSS12@7	434	303	23.1	0.70	0.0509	1.57	0.295	2.18	0.0421	1.51	234.4	35.9	262.5	5.1	265.7	3.9
HSS12@8	1254	1412	77.2	1.13	0.0526	0.93	0.318	1.78	0.0438	1.51	313.3	21.0	280.1	4.4	276.2	4.1
HSS12@9	398	279	22.4	0.70	0.0506	1.77	0.310	2.32	0.0444	1.50	221.1	40.5	273.8	5.6	280.0	4.1
HSS12@10	765	740	44.3	0.97	0.0531	1.74	0.317	2.30	0.0433	1.51	335.2	38.9	279.6	5.6	273.0	4.0
HSS12@11	909	744	54.8	0.82	0.0524	1.42	0.335	2.08	0.0463	1.52	304.9	31.9	293.4	5.3	292.0	4.3
Gabbro																
09HSS6@1	79.8	74.0	5.11	0.93	0.0542	4.53	0.360	4.81	0.0481	1.60	380.1	98.8	311.9	13.0	302.8	4.7
09HSS6@2	71.4	78.7	5.12	1.10	0.0544	4.36	0.391	4.69	0.0521	1.72	387.3	95.1	335.0	13.5	327.5	5.5
09HSS6@3	96.3	93.5	6.57	0.97	0.0543	3.74	0.387	4.04	0.0517	1.55	383.2	81.8	332.2	11.5	325.0	4.9
09HSS6@4	260	354	18.4	1.37	0.0542	2.99	0.367	3.36	0.0491	1.53	378.1	65.9	317.4	9.2	309.1	4.6
09HSS6@5	77.6	76.3	5.32	0.98	0.0566	4.14	0.400	4.44	0.0513	1.61	475.6	89.0	341.9	13.0	322.6	5.1
09HSS6@6	138	132	9.71	0.96	0.0541	6.45	0.393	6.64	0.0527	1.55	374.0	139.0	336.3	19.2	330.8	5.0
09HSS6@7	130	118	8.54	0.91	0.0528	6.17	0.362	6.36	0.0498	1.52	318.9	134.6	313.9	17.3	313.2	4.7
09HSS6@8	98.4	65.8	6.23	0.67	0.0490	8.16	0.349	8.32	0.0517	1.61	146.7	181.0	304.2	22.1	325.1	5.1
09HSS6@9	101	52.5	6.41	0.52	0.0555	3.90	0.405	4.20	0.0529	1.58	432.6	84.5	345.0	12.4	332.2	5.1
09HSS6@10	60.8	77.3	4.54	1.27	0.0512	5.26	0.363	5.57	0.0514	1.83	252.0	116.7	314.4	15.2	322.9	5.8
09HSS6@11	62.4	37.6	3.84	0.60	0.0511	4.89	0.357	5.14	0.0508	1.59	243.2	108.9	310.3	13.8	319.3	4.9
09HSS6@12	78.8	65.9	5.44	0.84	0.0527	5.82	0.384	6.02	0.0528	1.57	317.9	127.0	329.7	17.1	331.4	5.1
09HSS6@13	131	139	9.05	1.06	0.0542	3.24	0.379	3.62	0.0507	1.61	377.7	71.2	326.2	10.1	319.0	5.0
09HSS6@14	70.1	50.8	4.47	0.72	0.0506	4.52	0.355	4.79	0.0509	1.58	220.8	101.3	308.6	12.8	320.3	4.9
09HSS6@15	174	172	11.9	0.99	0.0525	5.27	0.369	5.56	0.0510	1.77	308.3	115.7	318.9	15.3	320.4	5.5
09HSS6@16	119	97.1	8.10	0.82	0.0524	3.44	0.382	3.76	0.0529	1.52	304.7	76.4	328.7	10.6	332.1	4.9

Table 4
Hf–O isotopic data of zircons from volcanic and plutonic rocks in the Beishan region.

No.	Age (Ma)	$^{176}Lu/^{177}Hf$	$^{176}Hf/^{177}Hf$	$2\sigma_m$	$^{176}Hf/^{177}Hf_i$	$\varepsilon_{Hf}(0)$	$\varepsilon_{Hf}(t)$	T_{DM} (Ma)	$f_{Lu/Hf}$	$\delta^{18}O$	$2\sigma_m$
HSS6											
01	279.1	0.001463	0.282684	0.000030	0.282676	−3.1	2.8	815	−0.96	7.5	0.3
02	279.1	0.000816	0.282676	0.000022	0.282672	−3.4	2.6	813	−0.98	6.1	0.3
03	279.1	0.000924	0.282818	0.000022	0.282813	1.6	7.6	615	−0.97	6.8	0.3
04	279.1	0.003889	0.282844	0.000032	0.282823	2.5	8.0	628	−0.88	6.5	0.3
05	279.1	0.002201	0.282961	0.000028	0.282949	6.7	12.4	427	−0.93	7.6	0.3
06	279.1	0.000558	0.282609	0.000024	0.282606	−5.8	0.3	901	−0.98	6.2	0.3
07	279.1	0.002221	0.282839	0.000024	0.282827	2.4	8.1	606	−0.93	6.2	0.2
08										7.6	0.3
09										10.3	0.3
10	279.1	0.001145	0.282659	0.000031	0.282653	−4.0	1.9	844	−0.97	7.3	0.3
11	279.1	0.001226	0.282945	0.000035	0.282938	6.1	12.0	438	−0.96	7.0	0.4
12	279.1	0.006239	0.282871	0.000044	0.282838	3.5	8.5	629	−0.81	4.3	0.3
13										5.9	0.2
14	279.1	0.001223	0.282729	0.000038	0.282723	−1.5	4.4	746	−0.96	7.2	0.3
15										6.1	0.3
16	279.1	0.001342	0.283075	0.000063	0.283068	10.7	16.6	253	−0.96	5.3	0.3
17										4.9	0.4
18										5.9	0.3
19										6.4	0.3
20	279.1	0.002372	0.282753	0.000039	0.282740	−0.7	5.0	735	−0.93	5.6	0.3
HSS12											
01	279.7	0.002938	0.282671	0.000037	0.282656	−3.6	2.0	868	−0.91	7.7	0.4
02	279.7	0.002061	0.282642	0.000037	0.282631	−4.6	1.2	890	−0.94	7.5	0.3
03	279.7	0.005139	0.282800	0.000039	0.282773	1.0	6.2	720	−0.85	8.9	0.3
04	279.7	0.002176	0.282681	0.000040	0.282669	−3.2	2.5	836	−0.93	10.3	0.2
05	279.7	0.002542	0.282753	0.000038	0.282740	−0.7	5.0	738	−0.92	7.2	0.4
06	279.7	0.002554	0.282815	0.000037	0.282802	1.5	7.2	647	−0.92	6.9	0.3
07	279.7	0.003734	0.282723	0.000039	0.282704	−1.7	3.7	808	−0.89	8.1	0.4
08	279.7	0.002469	0.282634	0.000036	0.282621	−4.9	0.8	912	−0.93	7.2	0.5
09	279.7	0.001341	0.282733	0.000034	0.282726	−1.4	4.5	743	−0.96	7.3	0.4
10	279.7	0.002216	0.282653	0.000037	0.282642	−4.2	1.5	877	−0.93	8.0	0.4
11	279.7	0.003175	0.282710	0.000030	0.282694	−2.2	3.4	815	−0.90	7.4	0.4
12	279.7	0.002776	0.282668	0.000041	0.282653	−3.7	1.9	869	−0.92	6.6	0.3
13	279.7	0.002959	0.282792	0.000033	0.282776	0.7	6.3	689	−0.91	6.9	0.3
14	279.7	0.001588	0.282752	0.000038	0.282744	−0.7	5.2	720	−0.95	9.3	0.4
15	279.7	0.002929	0.282782	0.000040	0.282767	0.4	6.0	703	−0.91	7.0	0.3
16	279.7	0.001535	0.282719	0.000036	0.282711	−1.9	4.0	767	−0.95	7.3	0.2
17	279.7	0.002502	0.282831	0.000030	0.282818	2.1	7.8	622	−0.92	6.9	0.4
18										6.6	0.3
19										8.7	0.4
20	279.7	0.002177	0.282685	0.000037	0.282674	−3.1	2.7	830	−0.93	6.7	0.2
21	279.7	0.002426	0.282712	0.000042	0.282699	−2.1	3.6	796	−0.93	8.7	0.3

Note: $\varepsilon_{Hf}(t) = [^{176}Hf/^{177}Hf_Z/^{176}Hf/^{177}Hf_{CHUR}(t) - 1] \times 10{,}000$; $^{176}Hf/^{177}Hf_{CHUR}(t) = ^{176}Hf/^{177}Hf_{CHUR}(0) - ^{176}Lu/^{177}Hf_{CHUR} \times (e^{\lambda t} - 1)$; $T_{DM} = (1/\lambda) \times \ln[1 + (^{176}Hf/^{177}Hf_{DM} - ^{176}Hf/^{177}Hf_Z)/(^{176}Lu/^{177}Hf_{DM} - ^{176}Lu/^{177}Hf_Z)]$; $f_{Lu/Hf} = ^{176}Hf/^{177}Hf_Z/^{176}Lu/^{177}Hf_{CHUR} - 1$; where f_Z and f_{DM} are the $f_{Lu/Hf}$ values of the zircon sample and the depleted mantle; subscript Z = analyzed zircon sample, CHUR = chondritic uniform reservoir; DM = depleted mantle; $\lambda = 1.867 \times 10^{-11}$ year^{-1}, decay constant of ^{176}Lu; $^{176}Hf/^{177}Hf_{DM} = 0.28325$; $^{176}Lu/^{177}Hf_{DM} = 0.0384$; present-day $^{176}Hf/^{177}Hf_{CHUR}(0) = 0.282772$; $^{176}Hf/^{177}Hf_{CHUR} = 0.0332$. TDM represents the model age calculated from the measured $^{176}Hf/^{177}Hf$ and $^{176}Lu/^{177}Hf$ ratios of a zircon, giving a minimum limit for the crustal residence age of the hafnium in the zircon.

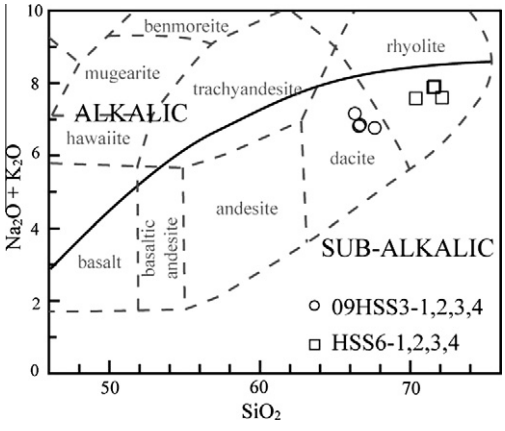

Fig. 4. Classification of volcanic rocks (after Cox et al., 1979).

and 90–863 ppm, respectively. They have Th/U ratios of 0.48–1.06, and a concordia age of 279.1 ± 2.9 Ma (MSWD = 0.25) (Table 3; Fig. 9). Their $\delta^{18}O$ values vary between +4.3 and +10.3), and their $^{176}Hf/^{177}Hf$ ratios range from 0.282609 to 0.282932, with corresponding $\varepsilon_{Hf}(t)$ values that fall between +0.3 and +8.5 (except one spot with $^{176}Hf/^{177}Hf = 0.283075$ and $\varepsilon_{Hf}(t) = +16.6$) (Table 4).

The Hongshishan diorite (HSS12) contains small zircon grains of 30–90 μm in length. These zircons are generally colorless and transparent to translucent. In CL imaging, most grains display regular concentric zoning with low luminescence while some have unzoned core and oscillatory zoned rims (Fig. 8). Eleven zircon grains from the Hongshishan diorite have large variations in U and Th contents of 210–1536 ppm and 114–1412 ppm respectively, and Th/U ratios of 0.54–1.16, yielding a mean age of 279.7 ± 4.8 Ma (MSWD = 3.0) (Table 3; Fig. 9). The $\delta^{18}O$ values and $^{176}Hf/^{177}Hf$ ratios of the zircons are between +6.6 and +10.3 and 0.282634–0.282831 respectively, with the latter corresponding to $\varepsilon_{Hf}(t)$ values in the range of +0.8 to +7.8 (Table 4).

Zircons in the Hongshishan gabbro (09HSS6) are mostly equant to long, prismatic and rarely occur as fragments. All the zircons are colorless and transparent, and range in length from 40 to 100 μm, with length/width ratios of 1:1–1.5:1. CL images of most zircons

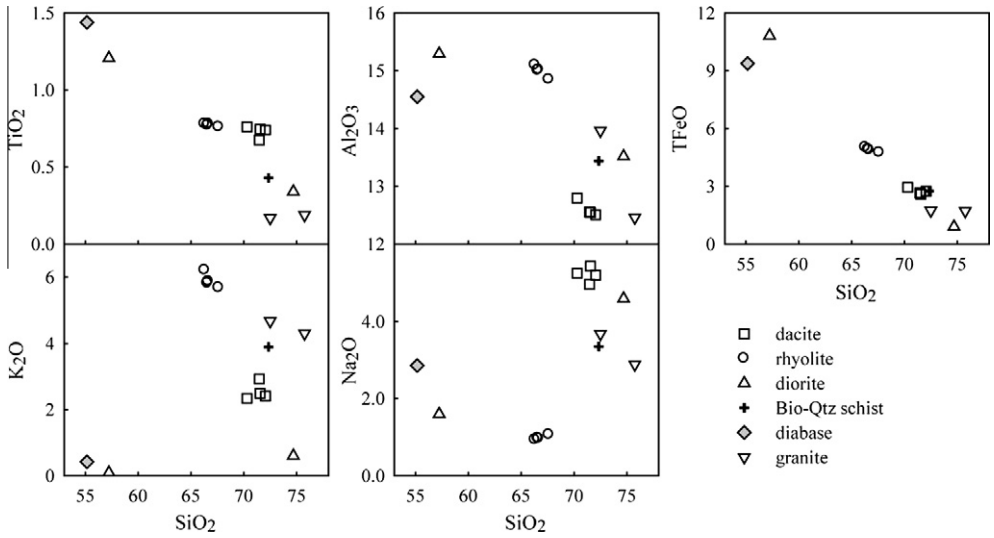

Fig. 5. Harker diagrams of SiO_2 versus TiO_2, Al_2O_3, TFeO (total Fe), K_2O and Na_2O of the investigated rocks from the Beishan region.

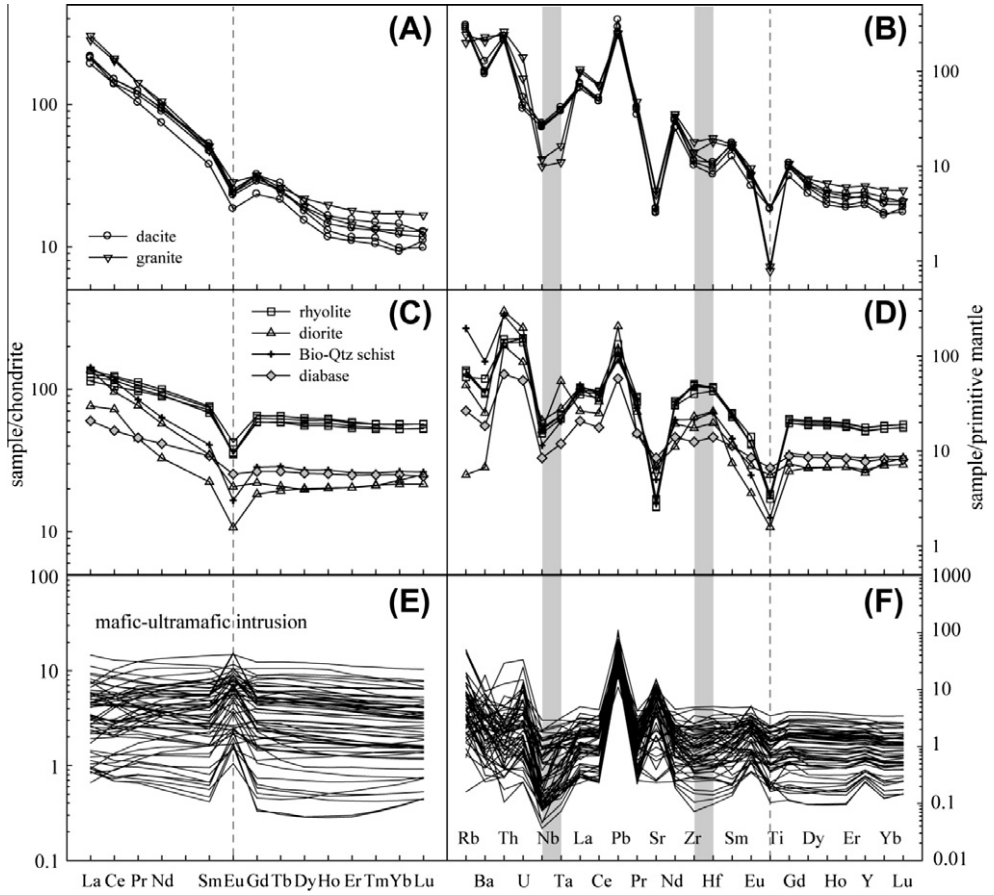

Fig. 6. Chondrite-normalized rare earth element and primitive mantle-normalized trace element patterns of the studied rocks and mafic–ultramafic intrusions from the Beishan region. Data of mafic–ultramafic complexes are from Jiang et al. (2006), Sun (2009) and Su et al. (2010c). Chondrite and primitive mantle values are from Anders and Grevesse (1989) and Sun and McDonough (1989), respectively.

display bright luminescence and apparent oscillatory zoned rims with low luminescence (Fig. 8). The zircons have U abundances in the range of 60.8–260 ppm, Th of 37.6–354 ppm, and Th/U ratios of 0.52–1.37 (Table 3). The concordia U–Pb age of sixteen analyzed zircons is 321.7 ± 3.4 Ma (MSWD = 1.11) (Fig. 9).

The zircons from the Hongshishan dacite (09HSS3) show large variations in morphology. They occur as fragments or round to long prismatic shapes with sizes in the range of 30–140 μm in length (Fig. 8). The zircons are colorless and transparent, and have large variations in U (58.4–511 ppm), and Th (31.9–633 ppm) with

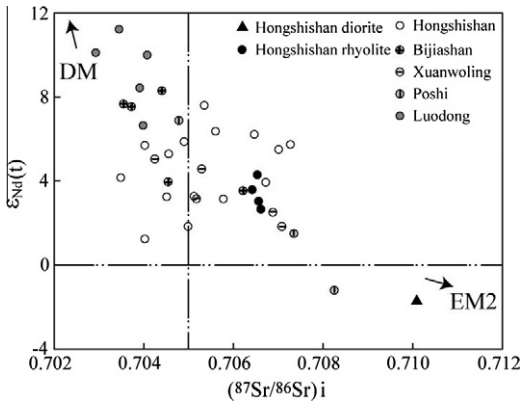

Fig. 7. $\varepsilon_{Nd}(t)$ vs. $(^{87}Sr/^{86}Sr)_i$ plot showing the Sr and Nd isotope compositions of the volcanic rocks and mafic–ultramafic intrusions from the Beishan region. All data have been adjusted to zircon U–Pb ages. Data sources: Jiang et al. (2006), Sun (2009) and Su et al. (2010c). DM, depleted mantle; EM2, enriched mantle 2; $\varepsilon_{Nd}(t) = 0$ and $(^{87}Sr/^{86}Sr)_i = 0.705$ are values of bulk silicate Earth (Zindler and Hart, 1986).

Th/U ratios of 0.28–1.62. $^{206}Pb/^{238}U$ ages of the zircons range from 265.1 Ma to 748.4 Ma (Table 3; Fig. 9).

5. Discussion

5.1. Carboniferous–Permian magmatic activities in the Beishan region

Several studies have shown that the southern margin of the COAB in NW China was in post-orogenic extensional setting in the late Paleozoic (e.g., Qin et al., 2002, 2003; Li et al., 2006b; Han et al., 2006; Wang et al., 2006). Mantle-derived magmatism was very active in the Eastern Tianshan and Beishan regions and produced a great number of mafic–ultramafic intrusions (Fig. 1B; Qin et al., 2002; Xu et al., 2009). Zircon U–Pb dating on the gabbro, norite and diorite in the Eastern Tianshan intrusions yielded the following ages: 277 Ma for Qiatertage (Li et al., 2006b), 285 Ma for Haibaotan (Li et al., 2006b), 269 Ma for Huangshanxi (Zhou et al., 2004), 284 Ma for Huangshan (Qin et al., in press), 274 Ma for Huangshandong (Han et al., 2004), 279 Ma for Xiangshan (Xiao et al., 2010b), 274 Ma for Hulu (Xia et al., 2008) and 301 Ma for Tulaergen (San et al., 2010). The zircons from Baishiquan and Tianyu gabbros in the Middle Tianshan Massif respectively have U–Pb ages of 281 Ma (Mao et al., 2006) and 280 Ma (Qin et al., in press). These geochronological studies revealed that the intrusions were mainly formed in the early Permian, and that the magmatic event in the Eastern Tianshan probably lasted from 300 Ma to 269 Ma or even later (Fig. 10; Qin et al., in press). However, very rare intermediate and acid igneous rocks, interpreted to have been formed in the early Permian occur in the Eastern Tianshan. These features suggest that mantle-derived magmatic activities were dominant in this region during the late Paleozoic.

Some previous isotopic and geochemical studies have demonstrated that Carboniferous–Permian magmatism was active in the Beishan region (e.g., Xiao et al., 2000, 2004a; Yang et al., 2008). Age dating of zircons in two gabbro samples from the Poshi intrusion yielded identical U–Pb ages of 274 Ma and 278 Ma (Li et al., 2006a; Jiang et al., 2006). Ao et al. (2010) reported zircon U–Pb ages of 282 Ma for the Hongshishan olivine gabbro and 271 Ma for the Poyi gabbro (Ao, 2010), while zircons from Poshi gabbro yielded U–Pb age of 284 Ma (Qin et al., in press). The zircons in gabbro from the Xuanwoling intrusion yielded U–Pb age of 261 Ma (Su et al., 2010a), whereas those from the Luodong and Bijiashan intrusions have U–Pb ages of 284 Ma and 279 Ma respectively (Fig. 10). These age data indicate that possible magmatic emplacements of most mafic–ultramafic intrusions were occurred around 280 Ma. The zircon U–Pb ages of the rhyolite (279 Ma) and diorite (280 Ma) suggest that ~280 Ma was also characterized by avtive acidic magmatism. The zircon U–Pb age of 322 Ma for the Carboniferous gabbro in the Hongshishan area (Figs. 2, 3A and 10) suggests that the mafic–ultramafic magmatic activities

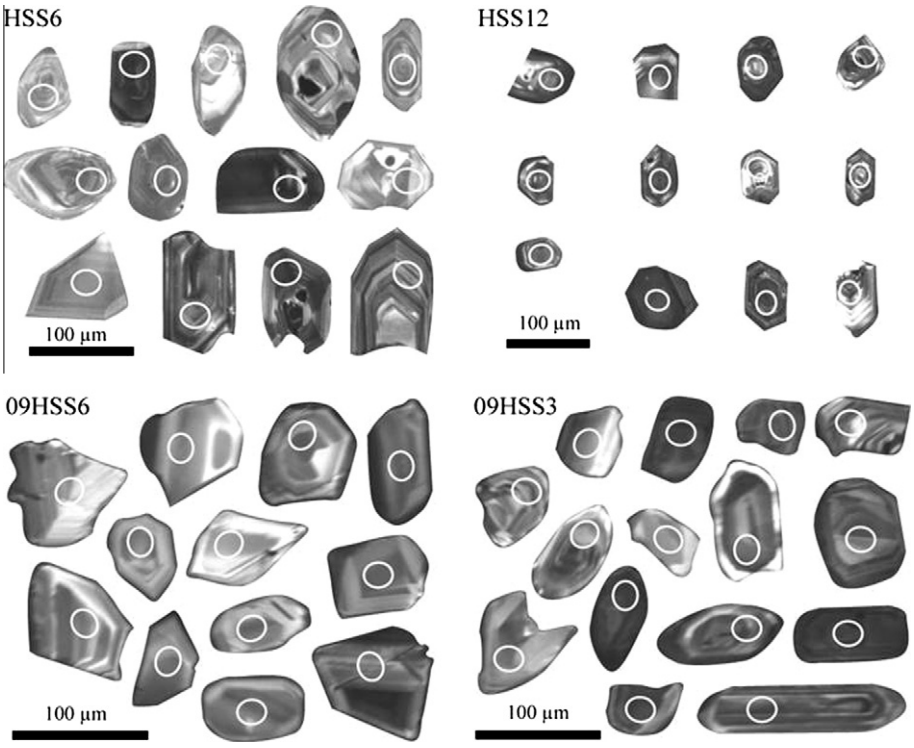

Fig. 8. CL images of representative zircons of the studied rocks from the Beishan region. Ellipses indicate the SIMS analyzing spots for U–Pb and O isotopes.

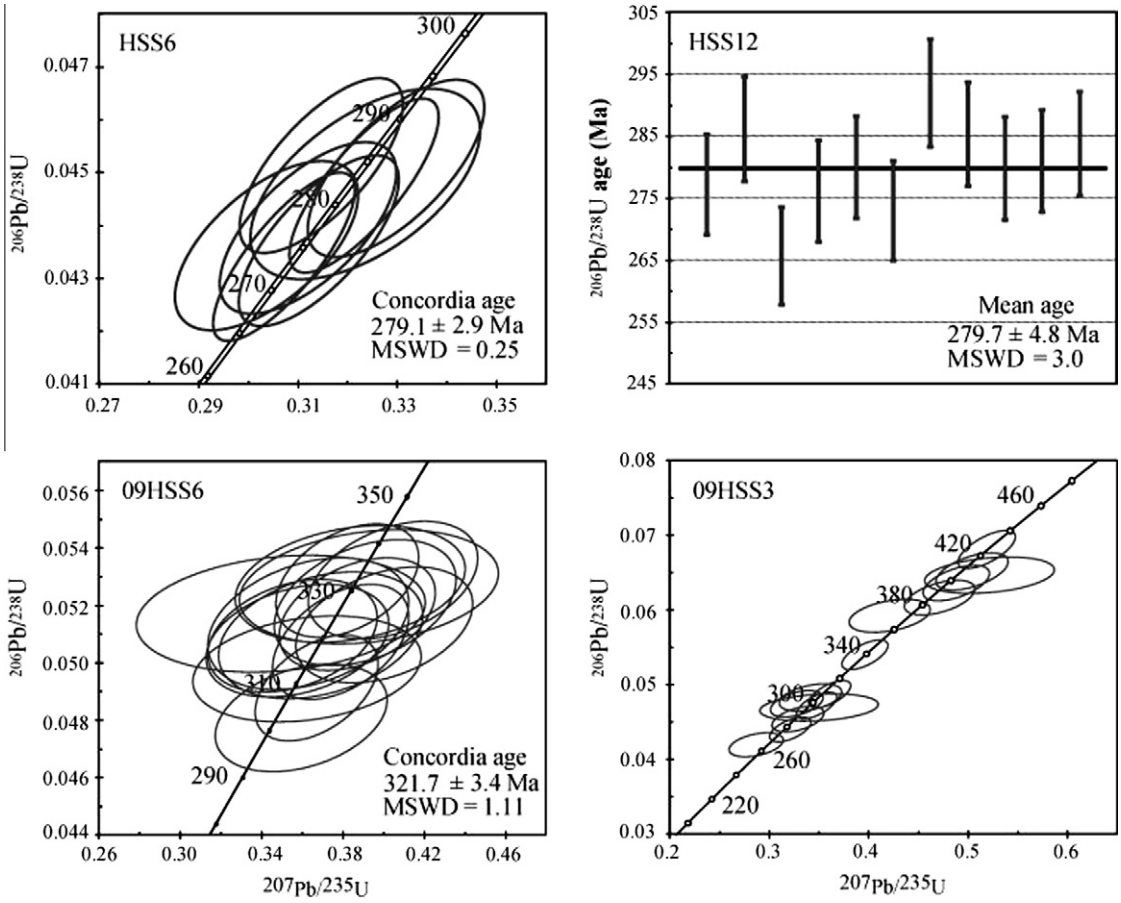

Fig. 9. Zircon U–Pb concordia plots of volcanic and intrusive rocks from the Beishan region. Data of HS139 are present in Su et al. (2010c).

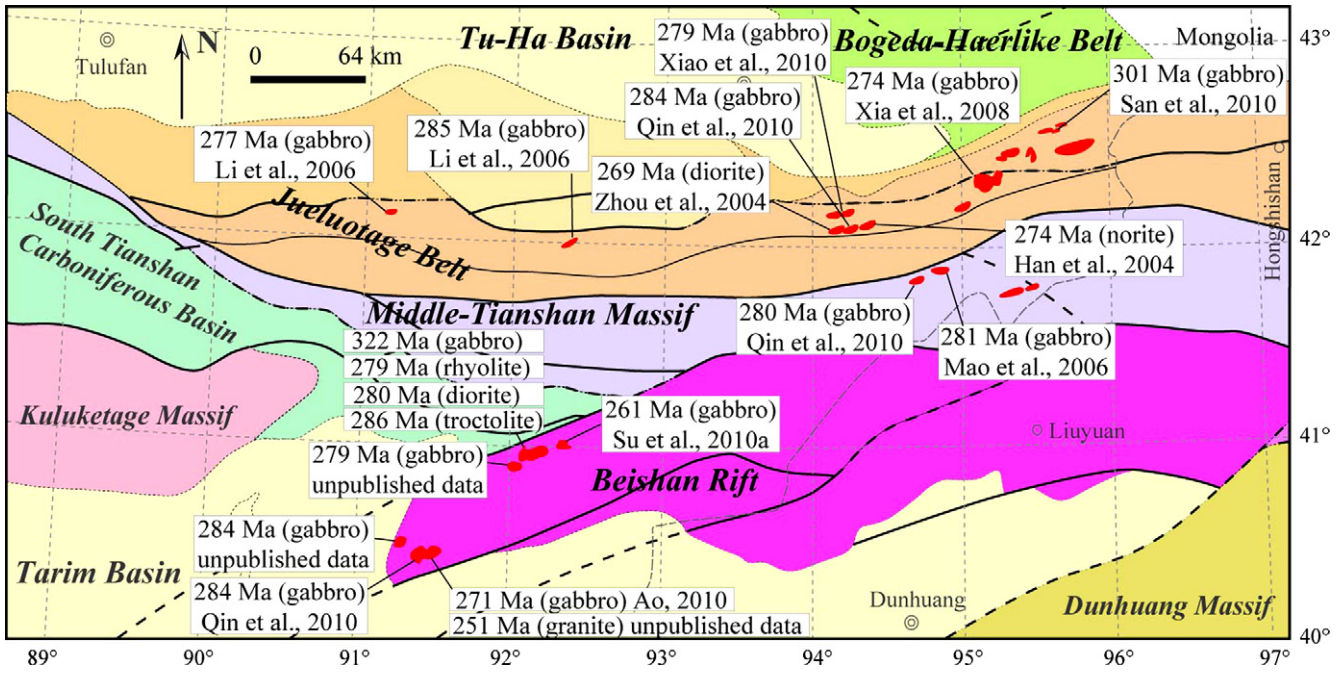

Fig. 10. Zircon U–Pb ages of the mafic–ultramafic intrusions and volcanic rocks in the Eastern Tianshan and Beishan regions. Data sources are illustrated on the map.

probably commenced from the Carboniferous. This is corroborated by Xiao et al. (2000, 2004a), who suggested that the Carboniferous granitic magmatism was widespread in the Beishan region, and the granites occurring as country rock of the Bijiashan intrusion are just the products of the Carboniferous magmatism. Therefore, the Carboniferous–Permian magmatic activities in the Beishan region

were dominated by abundant mafic–ultramafic intrusions, accompanied by acidic volcanic activities.

5.2. Petrogenesis of volcanic rocks

The mafic–ultramafic intrusions in the Beishan region are characterized by positive $\varepsilon_{Nd}(t)$ and zircon $\varepsilon_{Hf}(t)$ values, low ($^{87}Sr/^{86}Sr$)i values, generally flat REE patterns with negative Eu anomalies, enrichment in LILE and depletion in HFSE (Fig. 6E and F; Fig. 7; Jiang et al., 2006; Su et al., 2010a,c). These mafic–ultramafic complexes have been extensively studied and interpreted to be products evolving from high-Mg basaltic magmas derived from subduction-modified depleted mantle sources (Li et al., 2006a; Jiang et al., 2006; Mao et al., 2008; Pirajno et al., 2008; Su et al., 2009, 2010a,c). The CAOB is characterized by large volumes of Paleozoic and Mesozoic granitic intrusions as well as basaltic to rhyolitic rocks, all of which have features of positive $\varepsilon_{Nd}(t)$ values, low initial Sr isotopic ratios, and young Sm–Nd model ages of 300–1200 Ma (Hu et al., 2000; Jahn et al., 2000, 2004; Windley et al., 2007). These isotopic compositions point to their "juvenile" character and suggest their derivation from source rocks or magmas separated from the upper mantle (Sengör et al., 1993, 2004; Hu et al., 2000; Jahn et al., 2000, 2004; Windley et al., 2007; Condie et al., 2009; Sun et al., 2008; Xiao et al., 2009).

The rhyolites have positive $\varepsilon_{Nd}(t)$ and zircon $\varepsilon_{Hf}(t)$ values (Fig. 7; Fig. 11A), similar to the mafic–ultramafic rocks reported by Ao et al. (2010), suggesting that they were probably derived from a depleted mantle source or juvenile crust (Wu et al., 2007; Sun et al., 2008). Zircon Hf model ages of 427–901 Ma (Table 4), together with the distinct trace element abundances and normalized patterns between rhyolites and mafic–ultramafic intrusions (Fig. 6C and D) support a juvenile crust source for the rhyolites. The diorites and diabase have identical trace element patterns (Fig. 6C and D), positive zircon $\varepsilon_{Hf}(t)$ values and formation ages close to that of the rhyolites (Fig. 9; Fig. 11A and B), indicating that they possibly originated from a similar magma source. The LREE enrichments in the diorites and diabase with negative Eu anomalies and apparent Sr depletion (Fig. 6C and D) imply fractional crystallization of plagioclase. High $^{87}Sr/^{86}Sr$ values (Fig. 7) and particularly higher zircon $\delta^{18}O‰$ values than normal mantle zircons (5.3‰ ± 0.3‰) (Valley et al., 1998) (Fig. 11C and D) indicate crustal contamination in the petrogenesis of the diorite and diabase. The large variations of positive $\varepsilon_{Hf}(t)$ of the zircons and positive bulk $\varepsilon_{Nd}(t)$ further suggest that they had been subjected to variable degrees of crustal contamination. These geochemical features imply that the rhyolites, diorites and diabases were derived from juvenile crust sources, and subsequently experienced fractional crystallization and crustal contamination. The recent occurrence of juvenile crust in the Eastern Tianshan is restricted to the Late Devonian to Carboniferous only (e.g., Gu et al., 2001; Wang et al., 2006), whereas the present study confirms crustal growth events in the Beishan region in the Carboniferous and Permian.

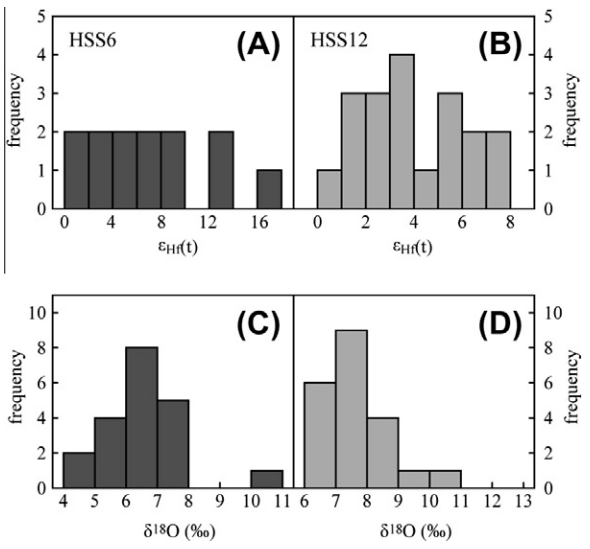

Fig. 11. Histograms of $\varepsilon_{Hf}(t)$ and $\delta^{18}O‰$ of zircons from the rhyolite (HSS6) and diorite (HSS12).

The dacites display trace element abundance and patterns that are identical to the Carboniferous granites from the Bijiashan (Fig. 6). Their extremely high $^{87}Sr/^{86}Sr$ values and low $^{143}Nd/^{144}Nd$ values (Table 2) indicate that they were most likely derived from older lower continental crust, which is consistent with the Precambrian crystalline basement in the Beishan region (BGMRXUAR, 1993; Qin et al., 2002; Xu et al., 2009). Significant crustal contamination during the ascent of the dacitic magmas are evidenced by abundant zircon grains having $^{206}Pb/^{238}U$ ages of 265–748 Ma (Table 3; Fig. 9).

5.3. Tectonic implications

The tectonic features of the Beishan region in the Permian have remained the subject of debate over the years. Some authors regard the mafic–ultramafic complexes as an Alaskan-type, thus they proposed that the Beishan region was an arc above a subduction zone (Mao, 2008; Xiao et al., 2009; Ao et al., 2010). However, these intrusions could be distinguished from the Alaskan-type complexes based on petrological, mineralogical and geochemical features: for example, their enrichments in plagioclase and troctolite abundances, and lack of hornblende, magnetite and hornblendite, which are are not consistent with typical features of Alaskan-type complex (Su et al., 2009, 2010a,c). Alternatively, most authors have proposed that the Beishan rift developed during the period from the Carboniferous to Permian (Xiao et al., 2000, 2004a; Jiang et al., 2006; Yang et al., 2008; Su et al., 2009, 2010a; Xu et al., 2009). The majority of the ophiolites in the Beishan region are older than the Carboniferous (Yang et al., 2008; Mao, 2008; Ao, 2010), suggesting that the subduction event responsible for the formation of the ophiolites ended before Carboniferous. Notably, the intergrowth of fault sag and fault uplift in the Beishan region separate the pre-Permian sedimentary sequences (BGMRXUAR, 1993; Xu et al., 2009; Qin et al., in press), which supports the model for rift developing in the Permian. However, bimodal volcanic rocks, a typical feature presents in most rifts worldwide, have not been reported so far in the Beishan region. The Hongshishan mafic–ultramafic complex is interpreted to represent tholeiitic basalts derived from mantle sources (Su et al., 2009; Ao et al., 2010). The outcrops of rhyolites in the west of the intrusion could represent crust-derived magmas. The formation or eruptive ages (~280 Ma) of the acidic volcanic rocks and mafic–ultramafic intrusions are the same within the analytical uncertainty and, therefore, could represent a litho-assemblage of "bimodal igneous rock", which further supports the premise that the Beishan region is a Permian rift.

The Tarim flood basalts have been identified as large igneous province related to the Permian mantle plume (Yang et al., 2007; Zhang et al., 2008; Chen et al., 2009; Zhou et al., 2009; Tian et al., 2010). Indeed, many large rifts have developed above mantle plumes, and typical examples are: the Afar plume and East African rift system (Rogers et al., 2000), the Emeishan plume and Panxi rift (Xu et al., 2001; He et al., 2003; Xiao et al., 2004b), and the Siberian plume and Baikal rift (Zorin et al., 2003; Saunders et al., 2005). Qin et al. (in press) discovered that the mafic–ultramafic intrusions in the Beishan Rift exhibit close geochronological and geochemical

correlations with the Tarim mafic intrusions and flood basalts. These hypotheses and comparisons suggest that the development of the Beishan Rift was most likely related to the Permian mantle plume event. The generation of Permian acidic magmas in the Beishan Rift is probably a crustal response to the mantle plume event which provided heat regime.

6. Conclusions

The Carboniferous–Permian magmatic activities in the Beishan region are dominated by mafic–ultramafic complexes, acidic intrusions and volcanic eruptions. The dacites were probably derived from older lower crustal materials and subsequently subjected to significant crustal assimilation, whereas the rhyolites (279 Ma), diorites (280 Ma) and diabases were most likely derived from juvenile crustal sources, which later experienced fractional crystallization and crustal contamination later on. The acidic igneous rocks and mafic–ultramafic complexes, which form bimodal igneous rock-type series, further support the hypothesis that the Beishan region was a Late Paleozoic rift probably developed in association with the early Permian mantle plume activity in the Tarim basin.

Acknowledgements

This study was financially supported by the Nature Science Foundation of China (Grant 41030424), Knowledge Innovation Program of the Chinese Academy of Sciences (Grant KZCX2-YW-107) and Chinese State 305 Program (Grant 2006BAB07B03-01). The authors would like to extend their gratitude to Li H., Jin X.D., Chu Z.Y., Li X.H., Tang G.Q. and Liu Y. for their assistance in geochemical and zircon analyses at the Institute of Geology and Geophysics, Chinese Academy of Sciences. The paper has benefited from constructive reviews by Prof. Bor-Ming Jahn and two anonymous reviewers.

References

Anders, E., Grevesse, N., 1989. Abundances of the elements: meteoritic and solar. Geochimica et Cosmochimica Acta 53, 197–214.

Ao, S.J., 2010. Paleozoic Accretionary Tectonics of the Beishan Orogen: Insights from Anatomy of Opiolites and Alaskan-type Complexes. PhD Thesis, Institute of Geology and Geophysics, Chinese Academy of Sciences (in Chinese with English abstract).

Ao, S.J., Xiao, W.J., Han, C.M., Mao, Q.G., Zhang, J.E., 2010. Geochronology and geochemistry of Early Permian mafic–ultramafic complexes in the Beishan area, Xinjiang, NW China: implications for late Paleozoic tectonic evolution of the southern Altaids. Gondwana Research 18, 466–478.

Bureau of Geology and Mineral Resources of Xinjiang Uygur Autonomous Region (BGMRXUAR), 1993. Regional Geology of Xinjiang Uygur Autonomous Region. Geological Publishing House, Beijing. pp. 1–841 (in Chinese).

Chen, H.L., Yang, S.F., Li, Z.L., Yu, X., Luo, J.C., He, G.Y., Lin, X.B., Wang, Q.H., 2009. Spatial and temporal characteristics of Permian large igneous province in Tarim Basin. Xinjiang Petroleum Geology 30, 179–182 (in Chinese with English abstract).

Chu, Z.Y., Wu, F.Y., Walker, R.J., Rudnick, R.L., Pitcher, L., Puchtel, I.S., Yang, Y.H., Wilde, S.A., 2009. Temporal evolution of the lithospheric mantle beneath the eastern North China Craton. Journal of Petrology. doi:10.1093/petrology/egp055.

Condie, K.C., Belousova, E., Griffin, W.L., Sircombe, K.N., 2009. Granitoid events in space and time: constraints from igneous and detrital zircon age spectra. Gondwana Research 15, 228–242.

Cox, K.G., Bell, J.D., Pankhurst, R.J., 1979. The interpretation of igneous rocks. George, Allen and Unwin, London.

Gao, J., Li, M.S., Xiao, X.C., Tang, Y.Q., He, G.Q., 1998. Paleozoic tectonic evolution of the Tianshan orogen, northwestern China. Tectonophysics 287, 213–231.

Gao, J., Long, L.L., Qian, Q., Huang, D.Z., Su, W., Klemd, R., 2006. South Tianshan: a late Paleozoic or a Triassic orogen. Acta Petrologica Sinica 22, 1049–1061 (in Chinese with English abstract).

Gao, J., Long, L.L., Klemd, R., Qian, Q., Liu, D.Y., Xiong, X.M., Su, W., Liu, W., Wang, Y.T., Yang, F.Q., 2009. Tectonic evolution of the South Tianshan orogen and adjacent regions, NW China: geochemical and age constraints of granitoid rocks. International Journal of Earth Sciences 98, 1221–1238.

Gu, L.X., Hu, S.X., Yu, C.S., Zhao, M., Wu, C.Z., Li, H.Y., 2001. Intrusive activities during compression–extension tectonic conversion in the Bogda intracontinental orogen. Acta Petrologica Sinica 17, 187–198 (in Chinese with English abstract).

Han, B.F., Ji, J.Q., Song, B., Chen, L.H., Li, Z.H., 2004. SHRIMP zircon U–Pb ages of Kalatongke No. 1 and Huangshandong Cu–Ni-bearing mafic–ultramafic complexes, North Xinjiang, and geological implications. Chinese Science Bulletin 49, 2424–2429.

Han, C.M., Xiao, W.J., Zhao, G.C., Mao, J.W., Li, S.Z., Yan, Z., Mao, Q.G., 2006. Major types, characteristics and geodynamic mechanism of upper Paleozoic copper deposits in northern Xinjiang, northwestern China. Ore Geology Reviews 28, 308–328.

He, B., Xu, Y.G., Chung, S.L., Xiao, L., Wang, Y.M., 2003. Sedimentary evidence for a rapid, kilometer-scale crustal doming prior to the eruption of the Emeishan flood basalts. Earth and Planetary Science Letters 213, 391–405.

Hu, A.Q., Jahn, B.M., Zhang, G., Chen, Y., Zhang, Q., 2000. Crustal evolution and Phanerozoic crustal growth in northern Xinjiang: Nd isotope evidence. 1. Isotopic characterization of basement rocks. Tectonophysics 328, 15–51.

Jahn, B.M., Wu, F., Chen, B., 2000. Grantoids of the Central Asian Orogenic Belt and continental growth in the Phanerozoic. Research of Society Edinburgh: Earth Science 91, 181–193.

Jahn, B.M., Windley, B., Natal'in, B., Dobretsov, N., 2004. Phanerozoic continental growth in Central Asia. Journal of Asian Earth Sciences 23, 599–603.

Jiang, C.Y., Cheng, S.L., Ye, S.F., Xia, M.Z., Jiang, H.B., Dai, Y.C., 2006. Lithogeochemistry and petrogenesis of Zhongposhanbei mafic rock body, at Beishan region, Xinjiang. Acta Petrologica Sinica 22, 115–126 (in Chinese with English abstract).

Li, H.Q., Chen, F.W., Mei, Y.P., Wu, H., Cheng, S.L., Yang, J.Q., Dai, Y.C., 2006a. Dating of the No. 1 intrusion of Pobei mafic–ultramafic rocks belt, Xinjiang, and its geological significance. Mineral Deposits 25, 463–469 (in Chinese with English abstract).

Li, J.Y., Song, B., Wang, K.Z., Li, Y.P., Sun, G.H., Qi, D.Y., 2006b. Permian mafic–ultramafic complexes on the southern margin of the Tu–Ha Basin, east Tianshan Mountains: geological records of vertical crustal growth in central Asia. Acta Geoscientica Sinica 27, 424–446 (in Chinese with English abstract).

Li, X.H., Liu, Y., Li, Q.L., Guo, C.H., Chamberlain, K.R., 2009. Precise determination of Phanerozoic zircon Pb/Pb age by multi-collector SIMS without external standardization. Geochemistry Geophysics Geosystem 10, Q04010. doi:10.1029/2009GC002400.

Li, X.H., Li, W.X., Li, Q.L., Wang, X.C., Liu, Y., Yang, Y.H., 2010a. Petrogenesis and tectonic significance of the 850 Ma Gangbian alkaline complex in South China: evidence from in situ zircon U–Pb dating, Hf–O isotopes and whole-rock geochemistry. Lithos 114, 1–15.

Li, J.Z., Wu, X.Z., Qi, X.F., Zhang, M., Zhang, Q.C., 2010b. Distribution and tectonic setting of upper Paleozoic volcanic rock in northern Xinjiang. Acta Petrologica Sinica 26, 195–206 (in Chinese with English abstract).

Long, L.L., Gao, J., Xiong, X.M., Qian, Q., 2006. The geochemical characteristics and the age of the Kule Lake ophiolite in the southern Tianshan. Acta Petrologica Sinica 22, 65–73 (in Chinese with English abstract).

Mao, Q.G., 2008. Paleozoic to Early Mesozoic Accretionary and Collisional Tectonics of the Beishan and Adjacent Area, Northwest China. PhD Thesis, Institute of Geology and Geophysics, Chinese Academy of Sciences (in Chinese with English abstract).

Mao, Q.G., Xiao, W.J., Han, C.M., Sun, M., Yuan, C., Yan, Z., Li, J.L., Yong, Y., Zhang, J.E., 2006. Zircon U–Pb age and geochemistry of the Baishiquan mafic–ultramafic complex in the Eastern Tianshan, Xinjiang: constraints on the closure of the Paleo-Asian Ocean. Acta Petrologica Sinica 22, 153–162 (in Chinese with English abstract).

Mao, J.W., Pirajno, F., Zhang, Z.H., Chai, F.M., Wu, H., Chen, S.P., Cheng, S.L., Yang, J.M., Zhang, C.Q., 2008. A review of the Cu–Ni sulfide deposits in the Chinese Tianshan and Altay orogens (Xinjiang Autonomous Region, NW China): principal characteristics and ore-forming processes. Journal of Asian Earth Sciences 32, 184–203.

Pirajno, F., Mao, J.W., Zhang, Z.C., Zhang, Z.H., Chai, F.M., 2008. The association of mafic–ultramafic intrusions and A-type magmatism in the Tianshan and Altay orogens, NW China: implications for geodynamic evolution and potential for the discovery of new ore deposits. Journal of Asian Earth Sciences 32, 165–183.

Qin, K.Z., Fang, T.H., Wang, S.L., 2002. Plate tectonics division, evolution and metallogenic settings in eastern Tianshan mountains, NW China. Xinjiang Geology 20, 302–308 (in Chinese with English abstract).

Qin, K.Z., Zhang, L.C., Xiao, W.J., Xu, X.W., Yan, Z., Mao, J.W., 2003. Overview of major Au, Cu, Ni and Fe deposits and metallogenic evolution of the eastern Tianshan Mountains, Northwestern China. In: Mao, J.W., Goldfarb, R.J., Seltmann R., Wang, D.W., Xiao, W.J., Hart, C. (Eds.), Tectonic Evolution and Metallogeny of the Chinese Altay and Tianshan, London, pp. 227–249.

Qin, K.Z., Su, B.X., Li, X.H., Tang, D.M., Sakyi, P.A., Sun, H., Xiao, Q.H., Liu, P.P., in press. SIMS zircon U–Pb geochronology and Sr–Nd isotopes of mafic–ultramafic intrusions in Eastern Tianshan and Beishan in correlation with flood basalts in Tarim Basin (NW China): constraints on a ca. 280 Ma mantle plume. American Journal of Sciences.

Rogers, N., Macdonald, R., Fitton, J.G., George, R., Smith, M., Barreiro, B., 2000. Two mantle plumes beneath the East African rift system: Sr, Nd and Pb isotope evidence from Kenya Rift basalts. Earth and Planetary Science Letters 176, 387–400.

San, J.Z., Qin, K.Z., Tang, Z.L., Tang, D.M., Su, B.X., Sun H., Xiao, Q.H., Liu, P.P., 2010. Precise zircon U–Pb age dating of two mafic–ultramafic complexes at Tulargen

large Cu–Ni district and its geological implications. Acta Petrologica Sinica 26, 3027–3035 (in Chinese with English abstract).
Saunders, A.D., England, R.W., Reichow, M.K., White, R.V., 2005. A mantle plume origin for the Siberian traps: uplift and extension in the West Siberian Basin, Russia. Lithos 79, 407–424.
Sengör, A.M.C., Natal'in, B.A., Burtman, V.S., 1993. Evolution of the Altaid tectonic collage and Paleozoic crustal growth in Asia. Nature 364, 299–307.
Sengör, A.M.C., Natal'in, B.A., Burtman, V.S., 2004. Phanerozoic analogues of Archean oceanic basement fragments: Altaid ophiolites and ophirags. In: Kusky, T.M. (Ed.), Precambrian Ophiolites and Related Rocks. Elsevier, Amsterdam, pp. 675–726.
Su, B.X., Qin, K.Z., Sun, H., Tang, D.M., Xiao, Q.H., Cao, M.J., 2009. Petrological and mineralogical characteristics of Hongshishan mafic–ultramafic complex in Beishan area, Xinjiang: implications for assimilation and fractional crystallization. Acta Petrologica Sinica 25, 873–887 (in Chinese with English abstract).
Su, B.X., Qin, K.Z., Sun, H., Wang, H., 2010a. Geochronological, petrological, mineralogical and geochemical studies of the Xuanwoling mafic–ultramafic intrusion in the Beishan area, Xinjiang. Acta Petrologica Sinica 26, 3283–3294 (in Chinese with English abstract).
Su, B.X., Qin, K.Z., Sakyi, P.A., Malaviarachchi, S.P.K., Liu, P.P., Tang, D.M., Xiao, Q.H., Sun, H., Ma, Y.G., Mao, Q., 2010b. Occurrence of an Alaskan-type complex in the Middle Tianshan Massif, Central Asian Orogenic Belt: Inferences from petrological and mineralogical studies. International Geology Review. doi:10.1080/00206814.2010.543009.
Su, B.X., Qin, K.Z., Sakyi, P.A., Tang, D.M., Liu, P.P., Malaviarachchi, S.P.K., Xiao, Q.H., Sun, H., 2010c. Geochronologic-petrochemical studies of the Hongshishan mafic–ultramafic intrusion, Beishan area, Xinjiang, NW China: petrogenesis and tectonic implications. International Geology Review. doi:10.1080/00206814.2010.543011.
Sun, H., 2009. Ore-forming Mechanism in Conduit System and Ore-bearing Property Evaluation for Mafic–Ultramafic Complex in Eastern Tianshan, Xinjiang. PhD Thesis, Institute of Geology and Geophysics, Chinese Academy of Sciences (in Chinese with English abstract).
Sun, S.S., McDonough, W.F., 1989. Chemical and isotopic systematic of oceanic basalts: implications for mantle composition and processes. In: Saunders, A.D., Norry, M.J. (Eds.), Magmatism in the Ocean Basins. Geological Society Special Publication. pp. 313–345.
Sun, M., Yuan, C., Xiao, W.J., Long, X.P., Xia, X.P., Zhao, G.C., Lin, S.F., Wu, F.Y., Kröner, A., 2008. Zircon U–Pb and Hf isotopic study of gneissic rocks from the Chinese Altai: progressive accretionary history in the early to middle Palaeozoic. Chemical Geology 247, 352–383.
Tang, D.M., Qin, K.Z., Sun, H., Su, B.X., Xiao, Q.H., Cheng, S.L., Li, J., 2009. Lithological, chronological and geochemical characteristics of Tianyu Cu–Ni deposit, East Tianshan: constraints on source and genesis of mafic–ultramafic intrusions in East Xinjiang. Acta Petrologica Sinica 25, 817–831 (in Chinese with English abstract).
Tian, W., Campbell, I.H., Allen, C.M., Guan, P., Pan, W.Q., Chen, M.M., Yu, H.J., Zhu, W.P., 2010. The Tarim picrite–basalt–rhyolite suite, a Permian flood basalt from northwest China with contrasting rhyolites produced by fractional crystallization and anatexis. Contributions to Mineralogy and Petrology. doi:10.1007/s00410-009-0485-3.
Valley, J.W., Kinny, P.D., Schulze, D.J., Spicuzza, M.J., 1998. Zircon megacrysts from kimberlite: oxygen isotope variability among mantle melts. Contributions to Mineralogy and Petrology 133, 1–11.
Wang, R.S., Wang, Y., Li, H.M., Zhou, D.W., Wang, J.L., 1998. Zircon U–Pb age and its geological significance of high-pressure terrane of granulite facies in Yushugou area, Southern Tianshan Mountain. Geochimica 27, 517–523 (in Chinese with English abstract).
Wang, J.B., Wang, Y.W., He, Z.J., 2006. Ore deposits as a guide to the tectonic evolution in the East Tianshan mountains, NW China. Geology in China 33, 461–469.
Windley, B.F., Alexeiev, D., Xiao, W.J., Kröner, A., Badarch, G., 2007. Tectonic models for accretion of the Central Asian Orogenic Belt. Journal of the Geological Society of London 164, 31–47.
Wu, F.Y., Yang, Y.H., Xie, L.W., Yang, J.H., Xu, P., 2006. Hf isotopic compositions of the standard zircons and baddeleyites used in U–Pb geochronology. Chemical Geology 234, 105–126.
Wu, F.Y., Li, X.H., Zheng, Y.F., Gao, S., 2007. Lu–Hf isotopic systematics and their applications in petrology. Acta Petrologica Sinica 23, 185–220 (in Chinese with English abstract).
Xia, M.Z., Jiang, C.Y., Qian, Z.Z., Sun, T., Xia, Z.D., Lu, R.H., 2008. Geochemistry and petrogenesis for Hulu intrusion in East Tianshan, Xinjiang. Acta Petrologica Sinica 24, 2749–2760 (in Chinese with English abstract).
Xiao, Y.F., Wang, D.Y., Wu, D.C., Deng, J.H., He, Z.W., 2000. Geological Evolution of the Western Beishan Tectonic Belt of Xinjiang. Sciences and Xinjiang, Publishing House of Science, Technology and Hygienc, Sichuan, pp. 113–139 (in Chinese).
Xiao, Y.F., Wang, D.Y., Deng, J.H., Sun, Y., Wu, D.C., 2004a. Volcanism during activity period of Beishan craton rift in Xinjiang, China. Journal of Chengdu University of Technology 31, 331–337.
Xiao, L., Xu, Y.G., Mei, H.J., Zheng, Y.F., He, B., Pirajno, F., 2004b. Distinct mantle sources of low-Ti and high-Ti basalts from the western Emeishan large igneous province, SW China: implications for plume–lithosphere interaction. Earth and Planetary Science Letters 228, 525–546.
Xiao, W.J., Windley, B.F., Yuan, C., Sun, M., Han, C.M., Lin, S.F., Chen, H.L., Yan, Q.R., Liu, D.Y., Qin, K.Z., Li, J.L., Sun, S., 2009. Paleozoic multiple subduction–accretion processes of the southern Altaids. American Journal of Science 309, 221–270.
Xiao, W.J., Huang, B.C., Han, C.M., Sun, S., Li, J.L., 2010a. A review of the western part of the Altaids: a key to understanding the architecture of accretionary orogens. Gondwana Research 18, 253–273.
Xiao, Q.H., Qin, K.Z., Tang, D.M., Su, B.X., Sun, H., San J.Z., Cao, M.J., Hui, W.D., 2010b. Xiangshan composite Cu–Ni–Ti–Fe and Ni–Cu deposit belongs to comagmatic evolution product: evidence from ore microscopy, zircon U–Pb chronology and petrological geochemistry, Hami, Xinjiang, NW China. Acta Petrologica Sinica 26, 503–522 (in Chinese with English abstract).
Xu, Y.G., Chung, S.L., Jahn, B.M., Wu, G.Y., 2001. Petrologic and geochemical constraints on the petrogenesis of Permian–Triassic Emeishan flood basalts in southwestern China. Lithos 58, 145–168.
Xu, X.Y., He, S.P., Wang, H.L., Chen, J.L., 2009. Geological Background Map of Mineralization in Eastern Tianshan–Beishan Area (in Chinese).
Yang, S.F., Li, Z.L., Chen, H.L., Santosh, M., Dong, C.W., Yu, X., 2007. Permian bimodal dyke of Tarim Basin, NW China: geochemical characteristics and tectonic implications. Gondwana Research 12, 113–120.
Yang, H.Q., Li, Y., Li, W.M., Yang, J.G., Zhao, G.B., Sun, N.Y., Wang, X.H., Tan, W.J., 2008. General discussion on metallogenetic tectonic setting of Beishan mountain, northwestern China. Northwestern Geology 41, 22–28 (in Chinese with English abstract).
Yue, Y.J., Liou, J.G., Graham, S.A., 2001. Tectonic correlation of Beishan and Inner Mongolia orogens and its implications for the palinspastic reconstruction of north China. In: Hendrix, M.S., Davis, G.A. (Eds.), Paleozoic and Mesozoic Tectonic Evolution of Central Asia: From Continental Assembly to Intracontinental Deformation, vol. 194. Geological Society of America Memoir, Boulder, Colorado, pp. 101–116.
Zhang, H.F., Sun, M., Lu, F.X., Zhou, X.H., Zhou, M.F., Liu, Y.S., Zhang, G.H., 2001. Geochemical significance of a garnet lherzolite from the Dahongshan kimberlite, Yangtze Craton, southern China. Geochemical Journal 35, 315–331.
Zhang, L.F., Ellis, D.J., Jiang, W., 2002. Ultrahigh pressure metamorphism in western Tianshan, China, part I: evidences from the inclusion of coesite pseudomorphs in garnet and quartz exsolution lamellae in omphacite in eclogites. American Mineralogist 87, 853–860.
Zhang, C.L., Li, X.H., Li, Z.X., Ye, H.M., Li, C.N., 2008. A Permian layered intrusive complex in the Western Tarim Block, northwestern China: product of a ca. 275 Ma mantle plume? The Journal of Geology 116, 269–287.
Zhou, M.F., Lesher, C.M., Yang, Z.X., Li, J.W., Sun, M., 2004. Geochemistry and petrogenesis of 270 Ma Ni–Cu-(PGE) sulfide-bearing mafic intrusions in the Huangshan district, Eastern Xinjiang, Northwest China: implications for the tectonic evolution of the Central Asian Orogenic Belt. Chemical Geology 209, 233–257.
Zhou, M.F., Zhao, J.H., Jiang, C.Y., Gao, J.F., Wang, W., Yang, S.H., 2009. OIB-like, heterogeneous mantle sources of Permian basaltic magmatism in the western Tarim Basin, NW China: implications for a possible Permian large igneous province. Lithos doi:10.1016/j.lithos.2009.06.027.
Zindler, A., Hart, S.R., 1986. Chemical geodynamics. Annual Review of Earth and Planetary Sciences 14, 493–571.
Zorin, Y.A., Turutanov, E.K., Mordvinova, V.V., Kozhevnikov, V.M., Yanovskaya, T.B., Treussov, A.V., 2003. The Baikal rift zone: the effect of mantle plumes on older structure. Tectonophysics 371, 153–173.